



Effect of bulk porosity on the pyroelectric properties of $\text{Na}_{0.5}\text{Bi}_{0.5}\text{TiO}_3\text{--}0.06\text{BaTiO}_3$ ceramics

Nishchay Saurabh¹ and Satyanarayan Patel^{1,*}

¹Department of Mechanical Engineering, Indian Institute of Technology Indore, Indore, Madhya Pradesh 453552, India

Received: 3 April 2023

Accepted: 21 May 2023

Published online:
2 June 2023

© The Author(s), under exclusive licence to Springer Science+Business Media, LLC, part of Springer Nature 2023

ABSTRACT

Numerous efforts have been made to improve the pyroelectric properties of lead-free ceramics through doping/substitution, nonstoichiometry, porosity and composite formation. Hence, the bulk porous $\text{Na}_{0.5}\text{Bi}_{0.5}\text{TiO}_3\text{--}0.06\text{BaTiO}_3$ (NBT–6BT) ceramics were prepared to obtain enhanced pyroelectric properties and figures of merit for energy harvesting. For this purpose, the burnt-out polymer technique was used to obtain the desired porosity via 0–12% poly(methyl methacrylate) polymer addition. The dielectric constant for the unpoled and poled samples decreased from 2215 to 422 and 790 to 221, respectively, as the porosity increased from 6 to 30%. The pyroelectric coefficient was also examined at room temperature to show an increment from 4.8 to 6.62×10^{-4} C/m² K with increasing porosity from 6 to 10%. Pyroelectric figures of merit, i.e., voltage responsivity ($\sim 47.16 \times 10^{-3}$ m²/C) and energy harvesting (~ 78.75 J/m³K²), were observed to be highest for NBT–6BT (2 wt% PMMA) at room temperature. The findings suggest that the porous structure can enhance the pyroelectric properties of lead-free ceramics.

Introduction

Pyroelectric materials have the potential to be used in a range of applications, including energy harvesting from waste heat [1–3], thermal sensors [4, 5] and infrared detectors [6]. The pyroelectric effect is a phenomenon where a material generates an electric charge in response to a temporal temperature change [7]. The requirement for temperature fluctuations compared to bulky heat sources in thermoelectric

material makes it an ideal method for energy harvesting or sensing [8]. However, pyroelectric energy harvesting is limited by its poor pyroelectric coefficient, low Curie temperature and higher dielectric constant [9, 10]. Researchers have made efforts to enhance the pyroelectric properties by doping/substitution [11, 12], nonstoichiometry [13, 14], composite formation [15–17] and single crystals [10, 18]. However, a similar improvement in pyroelectric energy harvesting capabilities can be obtained by introducing porosity [19, 20]. This physical

Handling Editor: Till Froemling.

Address correspondence to E-mail: spatel@iiti.ac.in

modification can decrease the material's specific heat capacity, leading to a better thermal response [20]. Moreover, the porous structure decreases the dielectric constant and can be a further add-on for energy harvesting capabilities [20, 21]. Although having an advantage of porosity, it is also restricted by poor mechanical properties and decreased pyroelectric coefficient (p) [20, 22]. In this regard, porosity can be used to tune the complex relation between the thermal, dielectric and p . Depending upon the electrical and thermal circuits employed, the selection of pyroelectric material can be obtained using different figures of merit (FOM) [23, 24]. Generally, FOMs such as current responsivity (F_i), voltage responsivity (F_v), energy harvesting (F_e) and modified energy harvesting (F_e^*) are defined for the comparison of pyroelectric material.

Porous pyroelectric materials have garnered significant interest in recent years, particularly in energy conversion and harvesting. In this direction, Zhang et al. [19] investigated $\text{Ba}_{0.67}\text{Sr}_{0.33}\text{TiO}_3$ with porosity from 1 to 9.6% and obtained an increased p from 50 to $80 \times 10^{-4} \text{ C/m}^2 \text{ }^\circ\text{C}$ and decreased dielectric constant from 2000 to 1000 at room temperature. Srikanth et al. [25] used porous $\text{BaSn}_{0.05}\text{Ti}_{0.95}\text{O}_3$ and showed the porous sample figures of merit F_v and F_e to increase by 77% and 160% compared to bulk. Porous $\text{Ba}_{0.85}\text{Ca}_{0.15}\text{Zr}_{0.1}\text{Ti}_{0.9}\text{O}_3$ was fabricated using different wt% of PMMA by Sharma et al. [26] and at 29% porosity, the dielectric constant at 5 kHz decreased from 3481 to 1117. Further, Zhang et al. [22] used aligned porosity in lead zirconate titanate and increased the compressive strength from 19 MPa (random porosity) to 35 MPa (aligned porosity). In this context, developing porous pyroelectric materials can revolutionize the development of sustainable and energy-efficient harvesting processes.

Lead-based materials are known to harm the environment and human health, making the development of lead-free a crucial alternative. In this direction, BaTiO_3 -based ceramics have significantly increased pyroelectric properties [19, 24, 25]. Moreover, $\text{Na}_{0.5}\text{Bi}_{0.5}\text{TiO}_3$ has been widely used by researchers for its superior piezoelectric properties accompanied by high Curie temperature [27, 28]. Hence, $\text{Na}_{0.5}\text{Bi}_{0.5}\text{TiO}_3$ -0.06 BaTiO_3 (NBT-6BT) lead-free pyroelectric material has attracted significant attention due to its relatively high piezoelectric constant (d_{33}), increased depolarization temperature and

enhanced pyroelectric properties [14, 29–31]. Zhu et al. [32] fabricated porous NBT-6BT using freeze casting having 3–1 type aligned pore. The d_{33} and strain were 182 pC/N and 0.042% at an electric field of 7 kV/mm. However, they do not investigate the pyroelectric properties of the porous NBT-6BT. Thus, porous NBT-6BT could be an efficient material for pyroelectric energy harvesting which is considered in the present work.

This study reports the dielectric, impedance, pyroelectric and energy harvesting capabilities of bulk porous NBT-6BT material. The bulk NBT-6BT ceramic samples have been investigated for porosity and pyroelectric properties. PMMA (poly(methyl methacrylate)) with different wt% was added to make porosity using burn-out polymer technique. The pores were bulk in range, and the effect of different wt% PMMA in NBT-6BT was analyzed.

Experimental method

Synthesis

The $0.94\text{Na}_{0.5}\text{Bi}_{0.5}\text{TiO}_3$ -0.06 BaTiO_3 (NBT-6BT) was prepared using a solid-state reaction. The raw powders of Na_2CO_3 (99.5%), Bi_2O_3 (99.975%), TiO_2 (99.6%) and BaCO_3 (99.8%) (all Alfa Aesar) were mixed in their stoichiometric ratio. The stoichiometrically weighed materials were mixed in the planetary ball in ethanol media for 12 h. The resultant mixture was calcined at 900 °C for 3 h at a 5 K/min heating rate in a closed alumina crucible. The powders obtained after calcination were re-milled for 6 h in an ethanol medium at 250 rpm to remove any bulk formation. The powder was dried at room temperature, and 5 wt% PVA solution was added. Pore former PMMA (2, 4, 8, 12 wt%) was mixed with the powder and milled by mortar-pestle to obtain a homogeneous mixture. The mixed powder was then pressed into 12 mm diameter pellets using a uniaxial compacting machine under 215 MPa. The green samples (before sintering) thickness and diameter were 1.54 mm and 12 mm, which decreased after sintering to 1.26 mm and 10 mm, respectively. The sample is grounded to make the surface plane parallel for further analysis and measurement. Thus, the final sample diameter of 10 mm and thickness of 1.05 mm is used for the dielectric, pyroelectric, ferroelectric and impedance measurement.

The sintering temperature was varied at a different heating rate between room temperature to 1160 °C to burn out the PMMA polymer. The temperature was initially raised up to 240 °C at a heating rate of 2 °C/min, then by 1 °C/min till 420 °C, followed by 2 °C/min till 850 °C, then by 5 °C/min up to 1160 °C. The sample was finally sintered at 1160 °C for 4 h and the furnace cooled. The sample $0.94\text{Na}_{0.5}\text{Bi}_{0.5}\text{TiO}_3-0.06\text{BaTiO}_3$, 2 wt% PMMA in NBT–6BT, 4 wt% PMMA in NBT–6BT, 8 wt% PMMA in NBT–6BT and 12 wt% PMMA in NBT–6BT are denoted by NBT–6BT Pure, NBT–6BT (2% PMMA), NBT–6BT (4% PMMA), NBT–6BT (8% PMMA) and NBT–6BT (12% PMMA).

Materials characterization and measurement

X-ray diffractometry (Empyrean, Malvern PANalytical, with Cu-K α radiation) was used to ascertain the phase of the material. Field emission scanning electron microscopy (FESEM, JEOL JSM-7610 plus) was used to observe the microstructure of the polished samples. The NBT–6BT pure samples were thermally etched at 1020 °C for 20 min to obtain an SEM micrograph. The density of the samples was measured using the Archimedes principle. The samples were electroded with silver paste on both sides and cured at 700 °C for 10 min. The samples were poled at 5 kV/mm at room temperature for 15 min. The poled and unpoled temperature-dependent dielectrics were measured using an LCR meter (NF Corp., ZM2376) in the 100 Hz–1 MHz frequency range. The impedance spectroscopy measurements were done in the frequency and temperature range of 0.1 Hz–3 MHz and 350–600 °C, respectively (NF Corp., ZM2376). A Sawyer–Tower circuit was used to measure the temperature-dependent polarization (P – E) hysteresis loops at 1 Hz frequency using a triangular field. The temperature-dependent pyroelectric coefficient was measured using an electrometer (Keithley 6517B) at a 5 °C/min heating rate.

Results and discussion

The XRD pattern of the NBT–6BT pure, NBT–6BT (4% PMMA) and NBT–6BT (12% PMMA) is shown in Fig. 1. The XRD pattern was measured at room temperature in the 2θ range of 20–80°. The XRD reveals a single homogeneous perovskite structure.

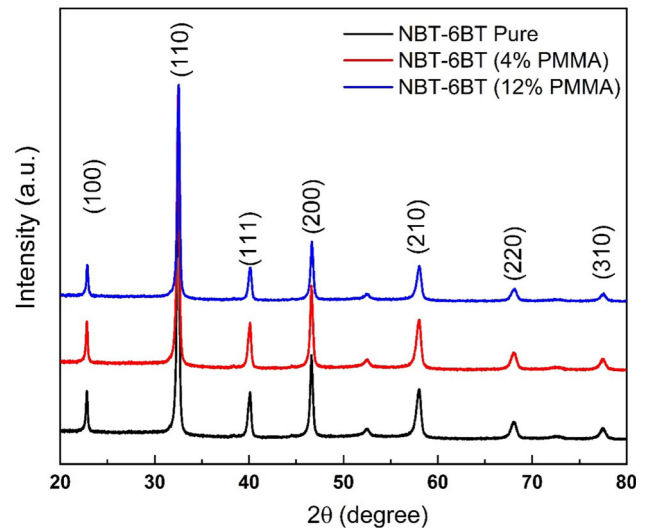


Figure 1 X-ray diffraction pattern for sintered ceramic samples.

The samples were indexed according to a single ABO_3 perovskite structure. The XRD patterns follow the work done by previous researchers [31, 33]. As no extra peaks could be observed in the XRD, the samples could be treated as phase pure.

The surface morphology of the ceramic samples with different wt% of PMMA is shown in Fig. 2. Thermal etching of pure NBT–6BT sample was responsible for grain growth and is visible in Fig. 2a. The porous samples were abstained from thermal etching as the grain growth would restrict the pore size and the interconnectivity between the pores. As the size of the PMMA taken was in the range of 200–300 μm , the relatively larger size of pores is obtained. It has been well known from the thermogravimetric analysis that PMMA starts burning at ~ 320 °C and is completely burnt at 400 °C. Thus, the varying heating rate during sintering resulted in the complete burning of PMMA. The vacant space was occupied by air and decreased the material density. The pores were observed to be well distributed throughout the surface. As the wt% of PMMA increases from 0 to 12%, the porosity of the sample increases from 6 to 30%.

The density (ρ) of the samples was measured using the Archimedes principle, and the porosity (P) of the samples was calculated using the following equation,

$$P = (\rho_{\text{Th}} - \rho_x) / \rho_{\text{Th}} \times 100\% \quad (1)$$

where ρ_{Th} is the theoretical density of the material and ρ_x is the density of the porous sample. The variation in porosity with the wt% of PMMA mixed

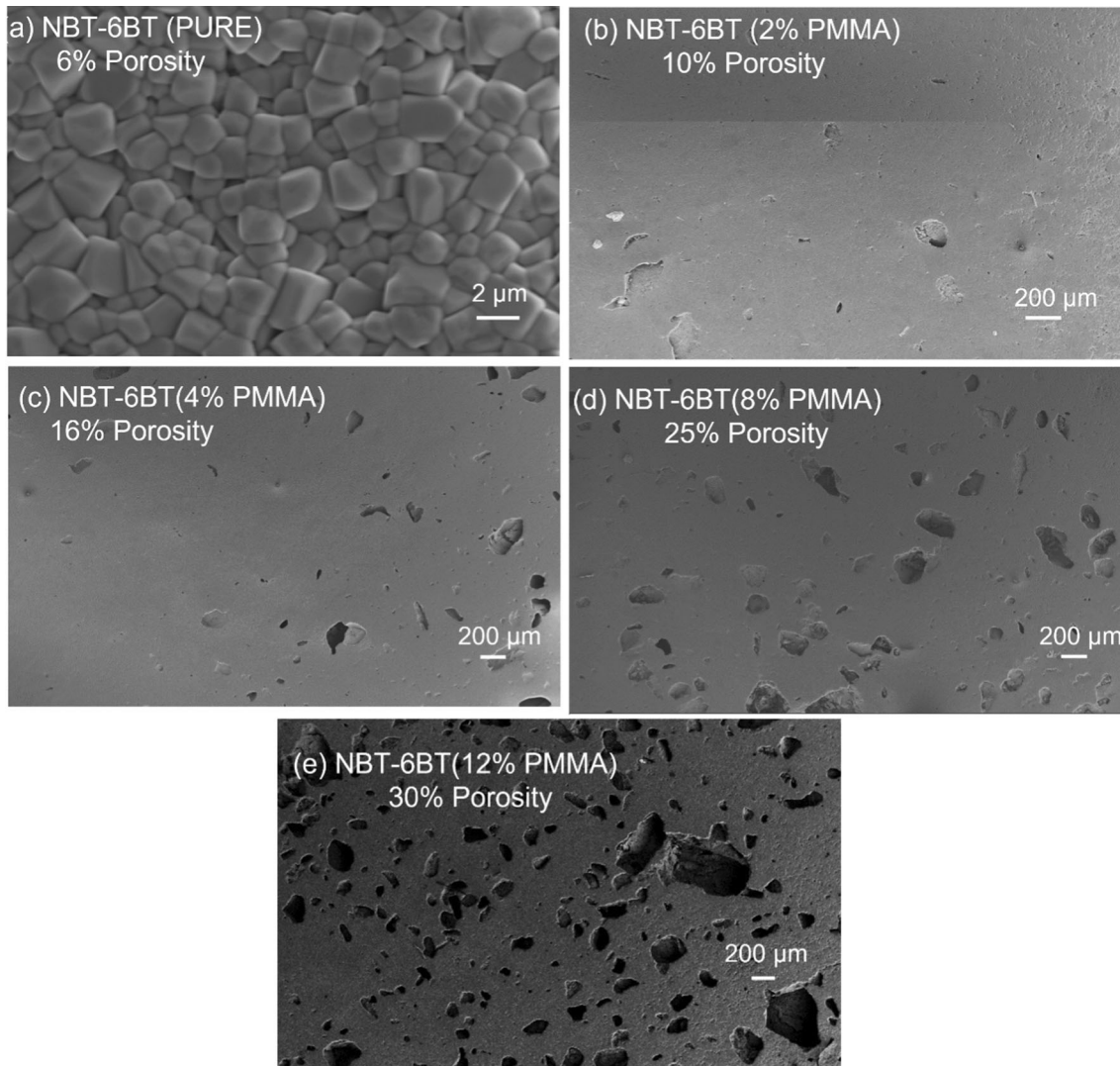


Figure 2 SEM images of the polished samples of **a** NBT–6BT Pure, **b** NBT–6BT (2% PMMA), **c** NBT–6BT (4% PMMA), **d** NBT–6BT (8% PMMA) and **e** NBT–6BT (12% PMMA).

is shown in Fig. 3. The theoretical density of the pure NBT–6BT material is taken to be 6200 g/cm^3 [14]. The density of the pure NBT–6BT sample is 5.818 g/cm^3 with a porosity of 6%. The density of the 12% PMMA in NBT–6BT was obtained as 4.381 gm/cm^3 . The porosity of the NBT–6BT pure, NBT–6BT (2% PMMA), NBT–6BT (4% PMMA), NBT–6BT (8% PMMA) and NBT–6BT (12% PMMA) were obtained to be 6%, 10%, 16%, 25% and 30%, respectively. The amount of PMMA can control the porosity content. The effect of porosity on Young’s modulus has been analyzed by Zeng et al. [34] on PZT ceramics. They found that the Young’s modulus decreased with porosity; thus, a decreased compressive strength was observed. Further, Zhang et al. [35] measured

compressive strength for pure and porous bulk PZT are $\sim 85 \text{ MPa}$ (pure) to $\sim 48 \text{ MPa}$ (20% porosity). The compressive strength decreases by $\sim 44\%$ compared to the pure sample. The Young’s modulus of bulk pure NBT–6BT is 122 MPa , two times higher than the bulk PZT (67 MPa) [36, 37]. Further, Wang et al. [37] reported that the fracture toughness and hardness of the NBT–6BT and PZT are $1.36 \text{ MPa m}^{1/2}$ and $0.82 \text{ MPa m}^{1/2}$ and 5.4 GPa and 3.0 GPa , respectively [36, 37]. Hence, the NBT–6BT porous sample’s compressive strength may also decrease similarly.

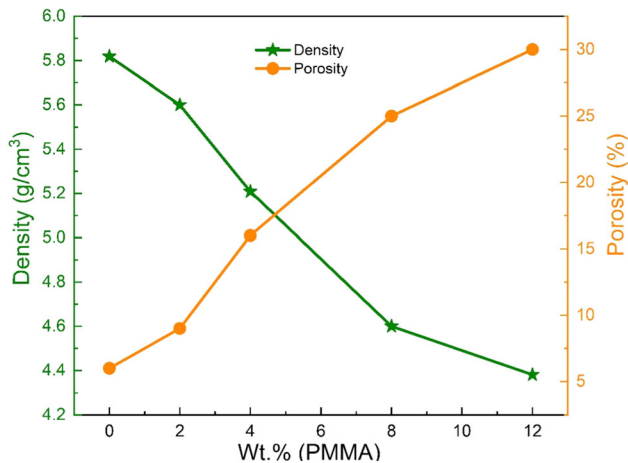


Figure 3 Variation of density and porosity with wt.% of PMMA added in NBT–6BT pure.

Effect of porosity on the dielectric behavior of the material

Figure 4 presents the temperature dependence of the dielectric constant and loss at various frequencies for unpoled samples of (a) pure NBT–6BT, (b) 2% PMMA, (c) 4% PMMA, (d) 8% PMMA and (e) 12% PMMA. The dielectric constant of the unpoled samples at room temperature decreased from 2215, 2100, 1748, 583 and 422 with an increase in porosity from 6 to 30% at room temperature. These results agree with their corresponding literature, which shows a steady decline in dielectric constant with porosity [20, 22, 26]. This is because porous materials are considered a two-phase system composed of pores and bulk ceramic material. The pores are filled with air with a dielectric constant of 1, and an effective dielectric constant of the porous sample can be found using any simple two-phase model. Using $\epsilon_{\text{eff}} = V_1 \epsilon_1 + V_2 \epsilon_2$, where V_1 and V_2 are the volume of bulk ceramic and pore and ϵ_1 and ϵ_2 are the dielectric constant of bulk ceramic and air, the dielectric constant of the porous sample can be calculated [19]. Thus, it is evident from the above expression that the extent of porosity can tailor the dielectric constant. Further, the presence of porosity can decrease the overall polarization of the material, which could be another reason for the decrease in the dielectric constant.

Small pores or voids may have a negligible effect on the dielectric behavior of the material, while larger pores or voids can have a more significant impact [38]. The shape of the pores can also affect the

dielectric behavior, with irregularly shaped pores being more detrimental to the dielectric constant than regularly shaped pores. Hence, the decrement in NBT–6BT (8% and 12% PMMA) is more pronounced. The distribution of the pores in the pyroelectric material can also play a role in its dielectric behavior. If the pores are evenly distributed throughout the material, the effect on the dielectric constant may be more uniform. The pyroelectric materials in the unpoled state show reduced pyroelectric properties. Thus, the bulk and porous samples are poled to enhance the pyroelectric property, where poling aligns the ferroelectric domains in the direction of the applied electric field.

The dielectric constant and loss for the poled samples are shown in Fig. 4f. The dielectric constant at room temperature for NBT–6BT pure, NBT–6BT (2% PMMA), NBT–6BT (4% PMMA) and NBT–6BT (8% PMMA) is measured to be 790, 628, 555 and 373. The poling effect is distinctly visible in Fig. 4f in the form of ferroelectric to relaxor phase transition at temperature $T_{\text{F-R}}$, which was clearly not found in the unpoled sample. The depolarization in NBT-based ceramics (including NBT–6BT) can be measured in two ways, distinguishing two stages in these ceramics [30, 39, 40]. First, temperature-dependent dielectric constant and loss measurement show a peak at ferroelectric–relaxor phase transition temperature, generally referred to as $T_{\text{F-R}}$. It is evident from Fig. 4f that a sharp peak in the poled sample is observed near 104 °C ($T_{\text{F-R}}$). In the second way/stage, the depolarization temperature (T_{d}) is observed in thermally stimulated depolarization current measurement. T_{d} is the temperature where macroscopic polarization of the material disappears, and a sharp increment in the temperature-induced current is obtained. Few studies suggest that T_{d} is 8 °C lower than $T_{\text{F-R}}$ [39, 41]. However, other studies do not clearly distinguish between T_{d} and $T_{\text{F-R}}$ [42]. Moreover, T_{d} and $T_{\text{F-R}}$ are always well below Curie temperature (T_{C}) [39, 41]. The measured $T_{\text{d}}/T_{\text{F-R}}$ and T_{C} from dielectric constant data of NBT–6BT are 104 °C and 250 °C, respectively; thus, the material depolarizes well below T_{C} . Salabaki et al. [3] have discussed the complete analysis of T_{d} , $T_{\text{F-R}}$ and T_{C} [43]. Many other researchers also have discussed T_{d} , $T_{\text{F-R}}$ and T_{C} in NBT–6BT and suggested that T_{d} should be used for piezoelectric and pyroelectric applications instead of T_{C} [14, 33, 44]. This is because, above $T_{\text{d}}/T_{\text{F-R}}$, the NBT-compositions have ferroelectric to relaxor phase

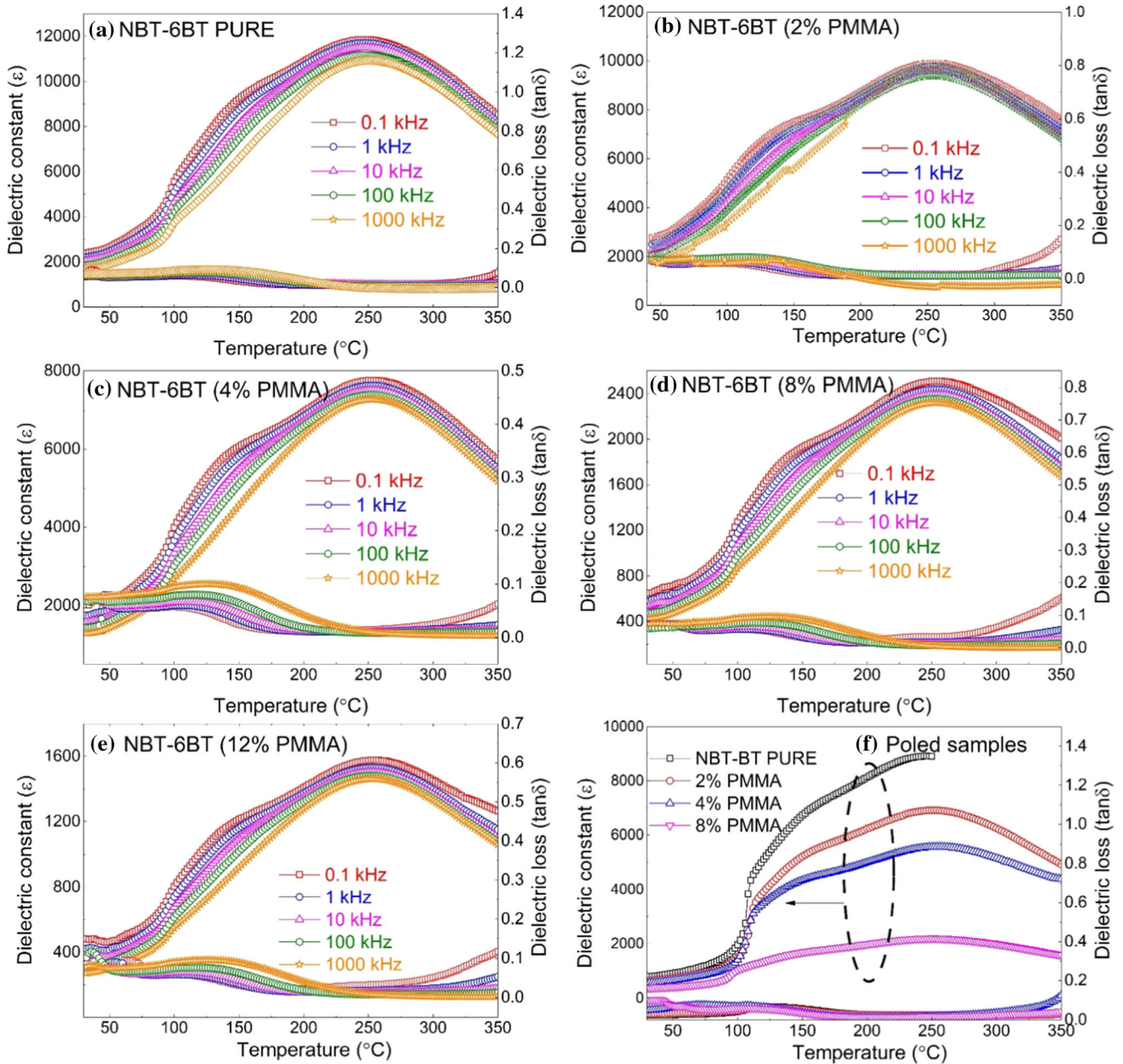


Figure 4 Comparison of temperature-dependent dielectric constant and dielectric loss for unpoled **a** NBT–6BT pure **b** NBT–6BTs (2% PMMA) **c** NBT–6BT (4% PMMA) **d** NBT–

6BT (8% PMMA) **e** NBT–6BT (12% PMMA) at frequency 0.1–1000 kHz and **f** dielectric constant and loss measured at 1 kHz frequency for poled bulk and porous samples.

transition accompanied by macroscopic depolarization. The NBT-based composition does not show pyroelectric and piezoelectric properties above T_d or T_{F-R} . Therefore, in the present work, T_d is considered for the pyroelectric analysis instead of the T_C .

Further, the sharp transition decreases with the decrease in effective poling in the case of 8% PMMA. The 12% PMMA sample could not be poled due to a large leakage current; therefore, the poled dielectric is

not shown in Fig. 4f. Hence, the poled dielectric constant and loss were used to calculate different figures of merit. The depolarization temperature (T_d) for the porous and bulk sample was obtained to be $\sim 104\text{--}105\text{ }^\circ\text{C}$, which shows that the effect of porosity on T_d is negligible. The poling effect can be observed in the $P\text{--}E$ loop, pyroelectric current density and figures of merit in the next sections.

Effect of porosity on P - E loop characteristics

Figure 5a shows virgin cycle (as fabricated sample: 1st cycle), 2nd cycle (unpoled sample) and poled sample P - E hysteresis loops at room temperature for NBT-6BT. As the positive polarity electric field is applied, large polarization response is observed in the virgin sample at about 3 MV/m; see Fig. 5a. This is because the electric field-induced phase transition occurs from the non-ergodic relaxor to the ferroelectric state accompanying domain switching [45, 46]. This ferroelectric phase is stable after field removal. Therefore, a large remanent polarization (P_{rem}) is obtained because of the irreversibility of phase transition and domain switching process. This can also be due to the high internal polarizability, strain and electromechanical coupling. P - E hysteresis loop of

the second cycle (Fig. 5a) indicates that the maximum polarization decreases compared to virgin samples. The reduction in P_{rem} from the 1st cycle to the 2nd cycle can be attributed to the absence of phase transformation strains. In order to achieve the virgin cycle polarization, the sample is poled, and the P - E hysteresis loop is measured, as shown in Fig. 5a. Thus, the poled sample has higher P_{rem} than the unpoled sample because poling has induced the electric non-ergodic relaxor to ferroelectric state phase transition accompanying the domain switching. Further, a similar coercive electric field (E_c) is obtained in the poled and unpoled 2nd cycle NBT-6BT. The poled and unpoled NBT-6BT (pure) sample dielectric constants are 2215 and 790, respectively, with ~ 3 orders of variation in dielectric constant

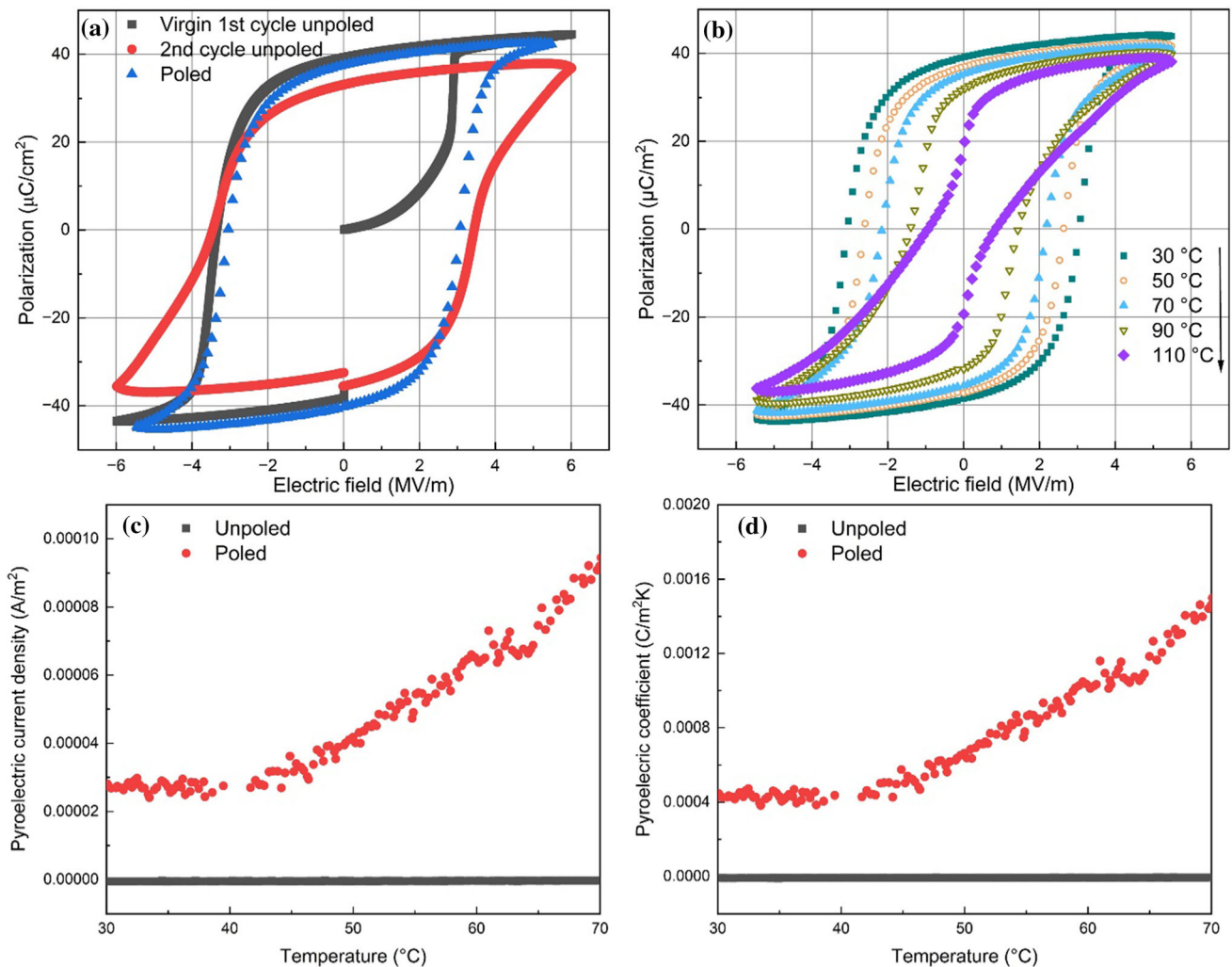


Figure 5 NBT-6BT pure bulk sample **a** P - E hysteresis loop of poled and unpoled samples, **b** P - E hysteresis loop at various temperatures, **c** pyroelectric current density and **d** pyroelectric coefficient.

results from electric field-induced phase transition (shown in Fig. 4f). Fig 5b shows the temperature-dependent P - E loops for the bulk NBT-6BT. The normal P - E hysteresis loop at room temperature transforms to a pinch type at a higher temperature resulting from the ferroelectric to ergodic relaxor phase transition. The temperature is generally referred as T_d , where the pinched/relaxor P - E hysteresis loop is obtained. Fig 5b shows a T_d between 100 and 110 °C. Saurabh et al. [14] and Tae et al. [33] reported a similar P - E loop with a T_d of ~ 104 °C. The present analysis reports a T_d of 104 °C as obtained from the dielectric curve and pyroelectric current density. The porosity also affects the P_{rem} , P_{max} and E_c of NBT-6BT. In this direction, Zhu et al. [32] reported the aligned porosity (36% porous) effect on the piezoelectric and ferroelectric properties of NBT-6BT. They showed that the P_{rem} , P_{max} and E_c are slightly decreased from 37 $\mu\text{C}/\text{cm}^2$, 33 $\mu\text{C}/\text{cm}^2$ and 4.83 kV/mm (pure bulk) to 33.5 $\mu\text{C}/\text{cm}^2$, 30 $\mu\text{C}/\text{cm}^2$ and 4.56 kV/mm (36% porous bulk), respectively. Zhu et al. [32] measured polarization by the bound charge over the nominal surface area, keeping the same dimensions. However, porous samples' effective surface area increases, and the polarization values may be underestimated. Thus, a similar effect of porosity on the P_{rem} , P_{max} and E_c can be considered in the present work. Further, this work uses burnt-out polymer technology to produce porosity; thus, the decrement in pyroelectric properties may slightly vary from Zhu et al. [13]. In order to look at the poling effect in NBT-6BT, the pyroelectric current and coefficient are estimated for poled and unpoled samples, shown in Fig. 5c and d, respectively. The pyroelectric current and coefficient are 1000 times higher in poled compared to unpoled sample. Such a remarkable improvement in the pyroelectric current and coefficient enhancement results from the electric field (poling) induced phase transition and domain switching. Thus, the poled NBT-6BT sample consists of higher pyroelectric current density and coefficient, as shown in Fig. 5c and d.

Effect of porosity on impedance spectroscopy

The impedance spectroscopy data were measured from 0.1 Hz to 3 MHz in the temperature range of 500–610 °C. The pure and porous NBT-6BT data were used for Nyquist plots. Impedance imaginary

part (Z'') vs. real part of impedance (Z') are shown in Fig. 6a–c for 500 °C, 550 °C and 610 °C. In pure and porous NBT-6BT, a single semicircle is observed at the measured temperature and frequency range, mainly due to the samples' bulk response. The bulk contribution was modeled using an equivalent circuit of resistance (R) connected in parallel with a constant phase element (CPE). The equivalent resistance can be observed to increase with porosity and overlap at higher temperatures. The samples conductivity was estimated using the relation $\sigma = t/(R \times A)$, where t , A and R give the thickness, cross-sectional area and resistance of the equivalent circuit. The temperature dependence conductivity also obeys the Arrhenius behavior given by

$$\sigma = \sigma_p \exp(-E_a/k_B T), \quad (2)$$

where k is the Boltzmann constant, E_a is the activation energy and σ_p is the pre-exponential factor.

The Arrhenius-type plot for NBT-6BT-type materials is fitted separately for high-temperature and low-temperature regions [14, 33]. The Arrhenius plot is fitted for high-temperature regions (550–610 °C) in the present analysis. The activation energy (E_a) of the sample material conduction process is obtained from the slope of the Arrhenius plot shown in Fig. 6d. The activation energy was obtained to be 1.56 eV, 1.63 eV, 1.64 eV, 1.62 eV and 1.63 eV for NBT-6BT Pure, NBT-6BT (2% PMMA), NBT-6BT (4% PMMA), NBT-6BT (8% PMMA) and NBT-6BT (12% PMMA). Regardless of the porosity, the activation energy of the samples was similar to the pure NBT-6BT. Thus, the conduction mechanism can be said to be independent of the porosity. This behavior of the porous pyroelectric materials would be helpful in pyro catalysis due to increased surface area. Although to analyze the effect of the energy harvesting capabilities of the porous materials, it is essential to look into pyroelectric properties and figure of merit.

Effect of porosity on the pyroelectric properties

Pyroelectric energy harvesting solely depends on the magnitude of current and voltage produced under an external temperature fluctuation. Theoretically, the magnitude of voltage produced depends on different parameters such as dielectric constant, sample thickness and temperature change [9]. The pore size distribution in the porous material is random in

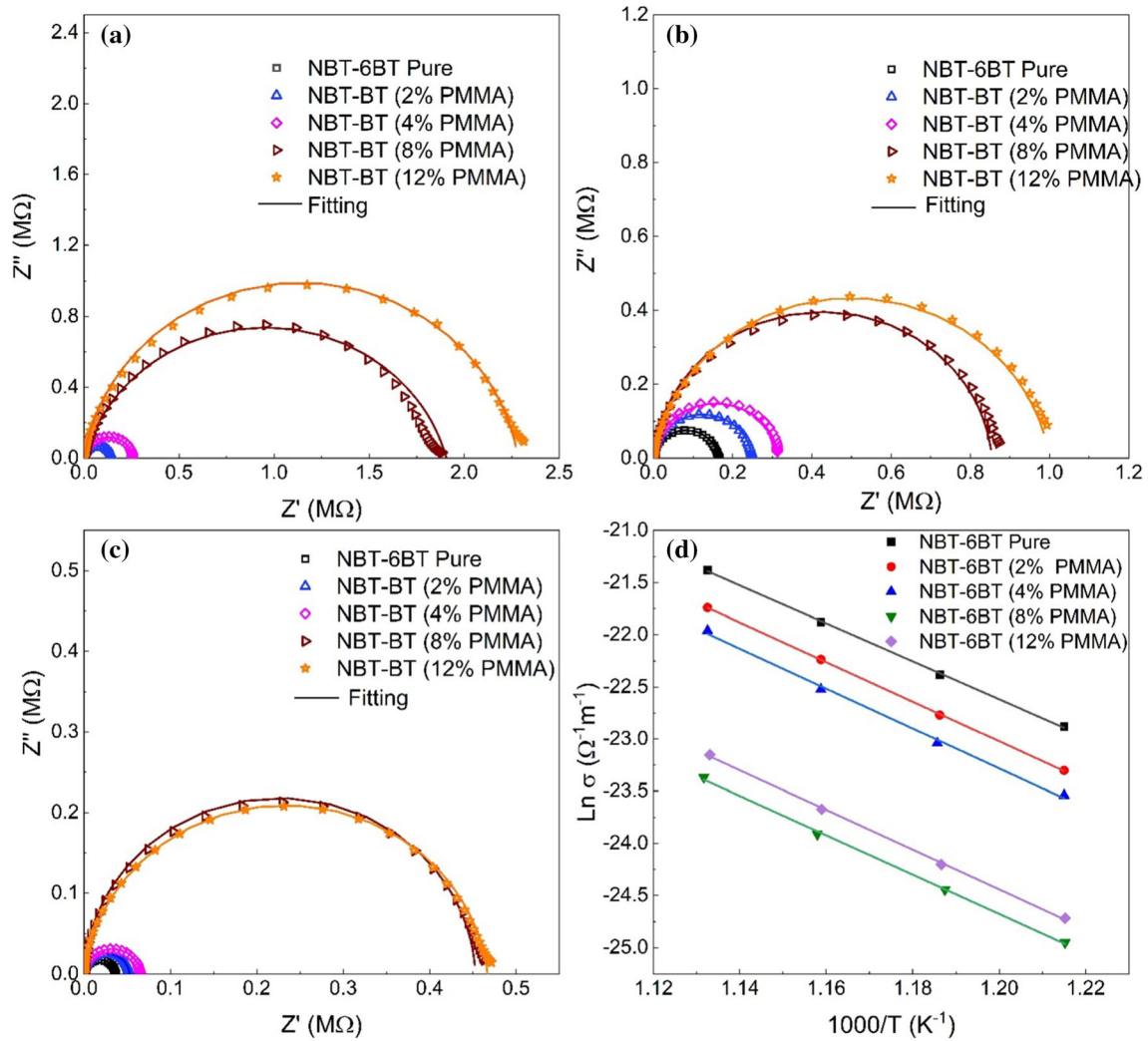


Figure 6 Nyquist plot (complex impedance plot) for NBT–6BT pure, NBT–6BT (2% PMMA), NBT–6BT (4% PMMA), NBT–6BT (8% PMMA) and NBT–6BT (12% PMMA) at **a** 510 °C,

b 550 °C, **c** 610 °C and **d** Arrhenius-type plot for bulk conductivity (high-temperature region).

nature, and the connectivity of the pores in the multiphase affects the material properties. In this regard, the random pores in the present analysis would be a good fit between the series and parallel model. For applying the series and parallel models in the current porous material, the 2–2 connectivity composite is assumed where the first phase is NBT–6BT and the second phase is the passive pore channel (denoted as ‘pc’, henceforth). The theoretical pyroelectric coefficient formulation for series connection [20, 47] is

$$p = \frac{V^{NBT-6BT} p^{NBT-6BT} \epsilon_{33}^{pc} + V^{pc} p^{pc} \epsilon_{33}^{NBT-6BT}}{V^{NBT-6BT} \epsilon_{33}^{pc} + V^{pc} \epsilon_{33}^{NBT-6BT}} + \frac{2V^{NBT-6BT} V^{pc} (\epsilon_{33}^{pc} \epsilon_{33}^{NBT-6BT} - \epsilon_{33}^{NBT-6BT} \epsilon_{33}^{pc}) (\alpha^{pc} - \alpha^{NBT-6BT})}{(V^{NBT-6BT} \epsilon_{33}^{pc} + V^{pc} \epsilon_{33}^{NBT-6BT}) [V^{NBT-6BT} (s_{11}^{pc} + s_{12}^{pc}) + V^{pc} (s_{11}^{NBT-6BT} + s_{12}^{NBT-6BT})]} \quad (3)$$

where p , V , ϵ , d , s , are pyroelectric coefficient, volume fraction, dielectric constant, piezoelectric coefficient and elastic compliance, respectively. If the pyroelectric, piezoelectric coefficient and elastic compliance of air are zero, zero and infinite, respectively. Then, above equation can be written as [20, 47]:

$$p = \frac{V^{NBT-6BT} p^{NBT-6BT}}{V^{NBT-6BT} + V^{pc} \times m} \quad (4)$$

where m is the ratio of dielectric constant of the two

phases $\epsilon_{33}^{\text{NBT-6BT}}/\epsilon_{33}^{\text{pc}}$. The pyroelectric coefficient for parallel connection can be written as:

$$p = V^{\text{NBT-6BT}} p^{\text{NBT-6BT}} + V^{\text{pc}} p^{\text{pc}} + \frac{V^{\text{NBT-6BT}} V^{\text{pc}} p^{\text{NBT-6BT}} (d_{33}^{\text{NBT-6BT}} - d_{33}^{\text{pc}}) (\alpha^{\text{pc}} - \alpha^{\text{NBT-6BT}})}{V^{\text{NBT-6BT}} \epsilon_{33}^{\text{pc}} + V^{\text{pc}} \epsilon_{33}^{\text{NBT-6BT}}} \quad (5)$$

Here, considering the above assumption (as used for Eq. 4) Eq. 5 can be written as

$$p = V^{\text{NBT-6BT}} p^{\text{NBT-6BT}} \quad (6)$$

However, these equations are valid for the aligned pores channels only. In this work pores are randomly distributed with nonuniform size (3–3 connected composite); hence, these models cannot be directly applied. Moreover, these models can provide a rough estimation for pyroelectric coefficient variation with porosity. Similarly, the current produced in open circuit conditions is directly proportional to the pyroelectric coefficient, rate of temperature change and cross-sectional surface area [9]. Factors such as the pyroelectric coefficient are intrinsic and cannot be altered with any physical alteration. However, there are numerous ways to structurally modify the material to improve p , including nonstoichiometry, chemical modification, composite formation, etc. [11–15] Following the theory and the associated equations shown in Fig. 7; there are only two ways to improve pyroelectric energy harvesting physically: first, by changing the design to increase A and h , and

second, by introducing porosity in the material. Under a fixed design consideration, porosity can enhance pyroelectric energy harvesting. The effect of porosity on the dielectric constant of the porous material is already seen in Fig. 4, where an increase in porosity was observed to decrease the dielectric constant. The impact of porosity on the pyroelectric current density and p is shown in Fig. 8.

Under a given boundary condition ($dT/dt = \text{const}$), the pyroelectric current density for a material depends on the silver coated (electroded) cross-sectional area (A) and p . For a porous material, with the increase in porosity, the A decreases and hence the I decrease. Further, with the introduction of porosity, the effective ferroelectric NBT–6BT phase decreases with a decrease in polarization. It can be concluded that the porous NBT–6BT materials have reduced ferroelectric domains compared to bulk NBT–6BT. Furthermore, the magnitude of p is also dependent on the effectiveness of the poling. Porous materials are difficult to pole due to higher leakage currents. As a combined result of the above reasons, the I of the pyroelectric material decreases with the porosity. Figure 8a shows the pyroelectric current density for bulk and porous NBT–6BT materials. Figure 8a and b inset depicts the variation of pyroelectric current density and p below the T_d , respectively. The temperature has been kept 20 °C below T_d to prevent the material from depolarization effects due to temperature overshooting in any practical application. In addition, cycling heating/cooling (10 cycles) is

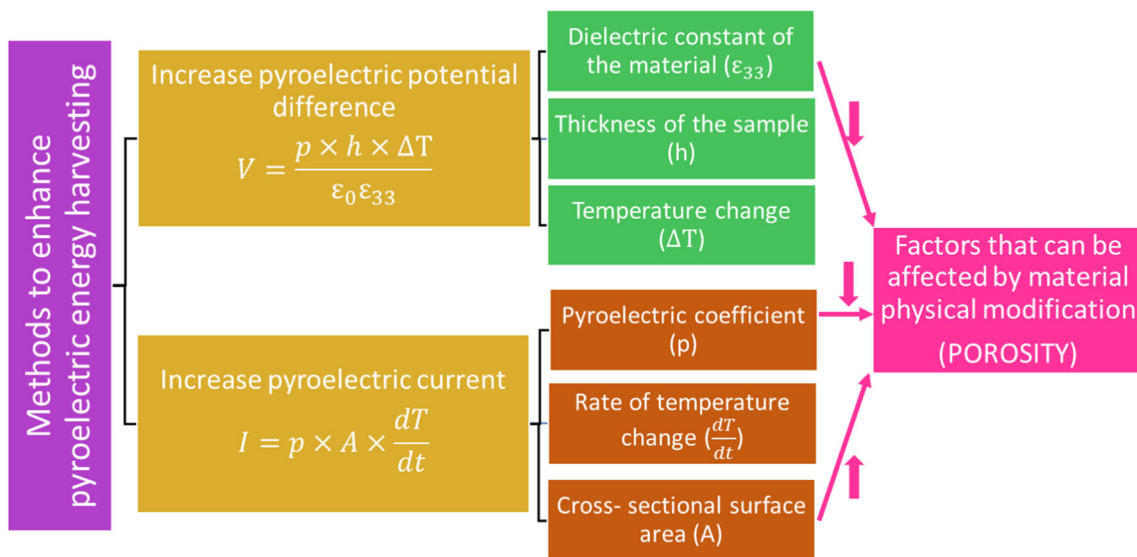


Figure 7 Schematic diagram showing the parameters affecting pyroelectric energy harvesting in bulk and porous samples.

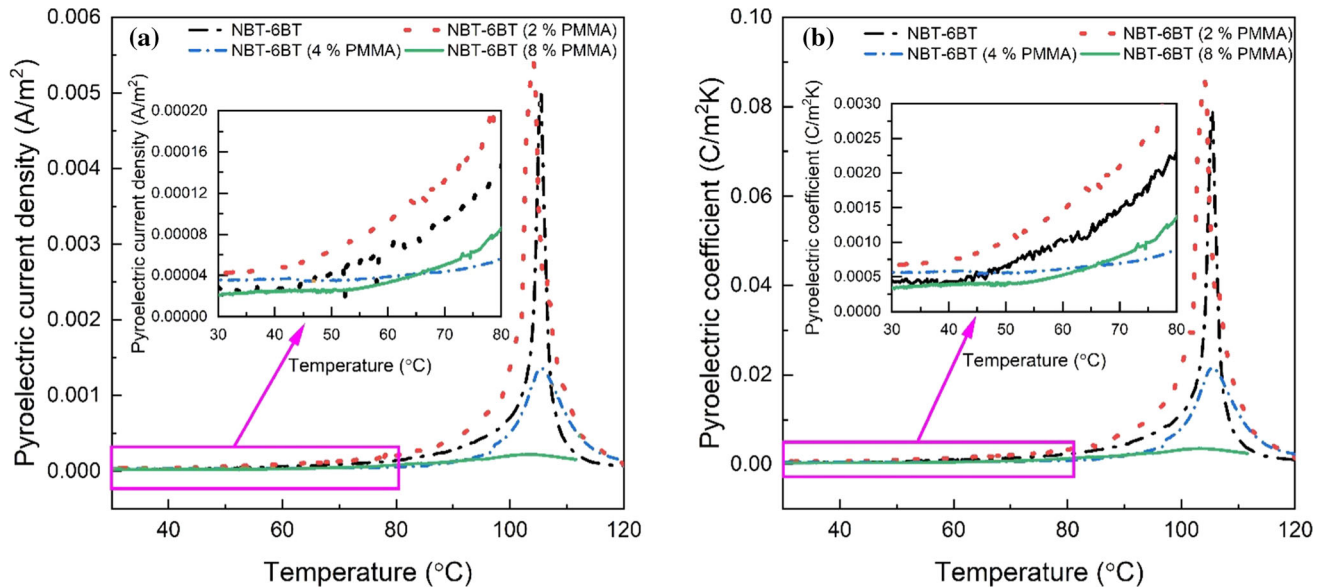


Figure 8 a Pyroelectric current density and b pyroelectric coefficient as a function of temperature for bulk and porous samples. The inset of figures shows the enlarged view of the pyroelectric current density and pyroelectric coefficient till 80 $^{\circ}C$.

performed to observe its effect on pyroelectric properties. The sample was held for 24 h after poling to avoid the domain switching's surface charge effect and relaxation before cyclic heating/cooling. It was observed that the pyroelectric current density and dielectric constant reduce by 5–8% at around room temperature and $\sim 30\%$ at 80 $^{\circ}C$ after the first cycle and later remain almost constant. Hence, the pyroelectric current density and coefficient in Fig. 8 are reported for the 10th cycle. In order to estimate figures of merit, the 10th cycle data of the dielectric constant and pyroelectric coefficient are used.

The T_d of the material is observed to be ~ 104 $^{\circ}C$ for bulk and porous samples. However, with the increase in porosity, the current peak at the T_d decreased. Although at room temperature, the pyroelectric current density (I/A) was obtained to be 2.85×10^{-5} A/m^2 , 3.81×10^{-5} A/m^2 , 4.55×10^{-5} A/m^2 and 2.1×10^{-5} A/m^2 for NBT-6BT pure, NBT-6BT (2% PMMA), NBT-6BT (4% PMMA) and NBT-6BT (8% PMMA). This increment in value for 2 and 4% PMMA in NBT-6BT may be due to higher interaction of temperature change due to increased overall surface area of interaction by porosity. However, in the case of NBT-6BT (8% PMMA), pyroelectric current density again decreases due to inefficient poling. In this regard, NBT-6BT (12% PMMA) could not be poled due to high leakage

current and increased porosity. The pyroelectric coefficient (p) has been calculated from the pyroelectric current density using the relation ($I = p \times A \times dT/dt$) as shown in Fig. 8b. A similar trend could also be observed for the pyroelectric coefficient. The pyroelectric coefficient at room temperature (30 $^{\circ}C$) was observed to be 4.38×10^{-4} $C/m^2 K$, 6.62×10^{-4} $C/m^2 K$, 5.64×10^{-4} $C/m^2 K$ and 3.3×10^{-4} $C/m^2 K$ NBT-6BT pure, NBT-6BT (2% PMMA), NBT-6BT (4% PMMA) and NBT-6BT (8% PMMA). This analogous behavior for an increase in p with porosity has also been reported by Srikanth et al. [25] and Zhang et al. [19]. Srikanth et al. [25] theoretically calculated the p for $BaSn_{0.05}Ti_{0.95}O_3$ with different amounts of PMMA added for porosity. The pyroelectric coefficient for $BaSn_{0.05}Ti_{0.95}O_3$ (0% PMMA), $BaSn_{0.05}Ti_{0.95}O_3$ (2% PMMA) and $BaSn_{0.05}Ti_{0.95}O_3$ (4% PMMA) was observed to be 4.32, 5.57 and 5×10^{-4} $C/m^2 K$. Similarly, Zhang et al. [19] at room temperature showed the p to increase from 50 to 80×10^{-4} $C/m^2 K$ when the porosity in $Ba_{0.67}Sr_{0.33}TiO_3$ was increased from 1 to 9.6%. At the lower porosity level, the decrease in ferroelectric domain due to porosity is overpowered by the lowered heat capacity (C_p), resulting in a better temperature change. This may be a primary reason for the increase in p at a temperature below T_d .

Effect of porosity on figures of merit of pyroelectric material

The ability of materials to generate energy for practical applications can be assessed by various figures of merit (FOM). These FOM contain a combination of physical properties to evaluate the pyroelectric material properties for energy harvesting. The variation of different FOM with temperature for a bulk and porous material is shown in Fig. 9. The current responsivity of the pyroelectric materials can be compared by the FOM $F_I = \frac{p}{\rho C_p}$, where ρ is the density of the material and C_p is the material's specific heat capacity. The C_p of the porous materials can be found using the relation [19] $C_p = C_{p(\text{dense})} \times (1 - \Phi)$, where Φ is the porosity fraction of the material. The C_p of the pure NBT-6BT material is taken to be 462 J/kg K [12, 14]. Higher

values of F_I are mainly used in infrared sensing devices. Figure 9a shows a 60% increment in F_I for 2% and 4% PMMA in NBT-6BT, while the 8% PMMA in NBT-6BT is similar to pure NBT-6BT at room temperature. In order to attain higher voltage responsivity for a given input power, FOM $F_V = \frac{p}{\rho C_p \epsilon \epsilon_0}$ should be enhanced. The F_V of all the porous materials was higher than the pure NBT-6BT. This is due to the dependency of F_V on p, ρ, C_p and ϵ . For 2 and 4% PMMA in NBT-6BT, the higher p and lower ρ, C_p and ϵ as compared to pure NBT-6BT were the sole reason for the increment. However, for 8% PMMA, although the p was lower than pure NBT-6BT, the value of ρ, C_p and ϵ was much lower. Hence, a combined effect resulted in an increment of F_V for 8% PMMA in NBT-6BT. Similarly, at 80 °C an increment of ~ 81% and 100 % was observed for 2 and 8% PMMA in F_V of NBT-6BT as compared to pure. A

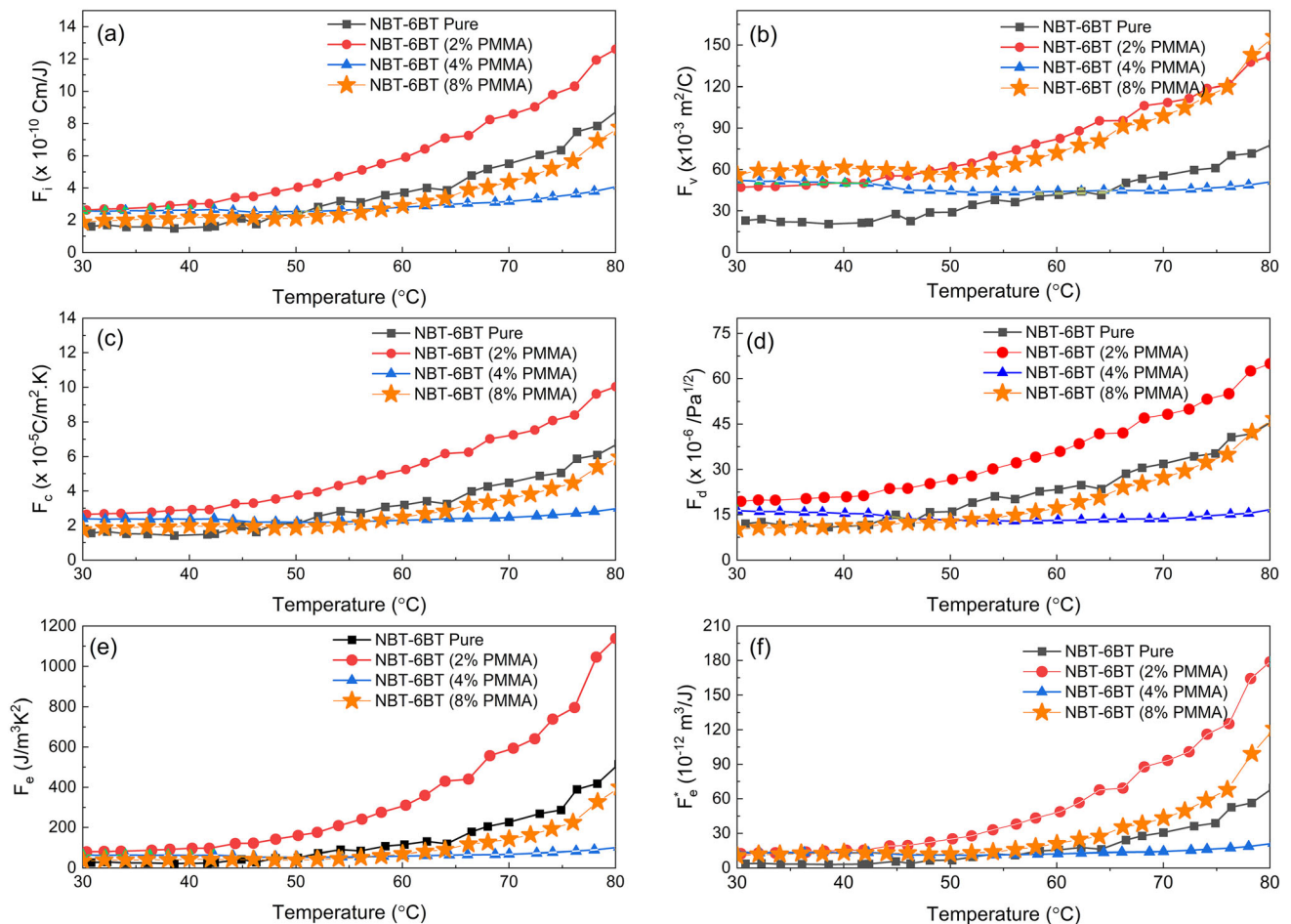


Figure 9 Pyroelectric figures of merit **a** F_I , **b** F_V , **c** F_c , **d** F_d , **e** F_e and **f** F_e^* as a function of temperature for pure and porous NBT-6BT samples.

Table 1 Comparison of pyroelectric coefficient and FOM of the present study with other well-known lead-free materials

Material	p ($\times 10^{-4}$ C/m ² K)	F_i ($\times 10^{-10}$ Cm/J)	F_v ($\times 10^{-3}$ m ² /C)	F_c ($\times 10^{-5}$ C/m ² .K)	F_d ($\times 10^{-6}$ /Pa ^{1/2})	F_e (J/ m ³ K ²)	F_e^* (10 ⁻¹² m ³ /J)	References
Ba _{0.85} Ca _{0.15} Zr _{0.1} Ti _{0.9} O ₃ (0% PMMA)	7.5	3.9	12	–	–	17.5	4.8	[26]
Ba _{0.85} Ca _{0.15} Zr _{0.1} Ti _{0.9} O ₃ (8% PMMA)	5	2.7	18	–	–	18.7	5.2	[26]
BaSn _{0.05} Ti _{0.95} O ₃ (2% PMMA)	5.57	3.55	18	–	–	8.2	2.34	[25]
Ba _{0.85} Sr _{0.15} Zr _{0.1} Ti _{0.9} O ₃ (5% PVA)	9.14	4.45	10	–	12.64	18.77	4.47	[24]
Ba _{0.85} Sr _{0.15} Zr _{0.1} Ti _{0.9} O ₃ (10% PVA)	8.54	4.42	11	–	13.25	18.51	4.97	[24]
Ba _{0.85} Sr _{0.15} Zr _{0.1} Ti _{0.9} O ₃ (15% PVA)	8.04	4.47	15	–	13.90	22.60	6.98	[24]
Polyvinylidene fluoride (PVDF)	2	0.8	8	–	–	4.2	0.6	[48]
0.005La–NBT–0.06BT–0.002Ta	12.92	4.61	78	2.57	2.76	–	–	[49]
(Ba _{0.84} Ca _{0.15} Sr _{0.01})(Ti _{0.90} Zr _{0.09} Sn _{0.01})O ₃	11.16	4.79	13	–	18.1	33.4	6.21	[50]
[Bi _{0.5} (Na _{0.95} K _{0.05}) _{0.5}] _{0.95} Ba _{0.05} TiO ₃	3.25	1.12	15	–	–	15.8	1.7	[51]
NBT–6BT pure	4.38	1.61	23.04	1.56	12	27.53	3.71	Present Study
NBT–6BT (2%PMMA)	6.62	2.62	47.16	2.64	19.38	78.75	12.38	Present Study
NBT–6BT (4%PMMA)	5.64	2.57	52.32	2.39	16.37	64.81	13.46	Present Study

similar behavior was observed for 4% PMMA in NBT–6BT, with almost constant FOM. This is mainly due to relatively constant p and ϵ in the temperature range of 30–80 °C.

Pyroelectric FOM F_c and high detectivity FOM F_d are defined as $(F_c) = \frac{p}{\sqrt{\epsilon}}$ and $(F_d) = \frac{p}{\rho c_p \sqrt{\epsilon \epsilon_0 \tan \delta}}$. An increment trend similar to F_i and F_v was also observed for F_c and F_d . At room temperature for NBT–6BT (2% PMMA), the F_c and F_d showed an increment of 69% (1.56 to 2.64×10^{-5} C/m.K) and 61% (12.02 – 19.38×10^6 /Pa^{1/2}) as compared to NBT–6BT pure. Further, thermal energy harvesting FOM $(F_e) = \frac{p^2}{\epsilon \epsilon_0}$ and $(F_e^*) = \frac{p^2}{\epsilon \epsilon_0 (\rho c_p)^2}$ is also calculated. The maximum F_e and F_e^* at room temperature and 80 °C are obtained to be 78.75 J/m³K² and 12.38×10^{-12} m³/J and 1137 J/m³K² and 178.94 m³/J for NBT–6BT (2% PMMA). A comparison of FOM with the available literature (selected materials) and present work for various lead-free materials is shown in Table 1. The comparison shows that porous NBT–6BT can be a good choice among various lead-free materials for energy harvesting.

The I – V measurement was carried out for practical energy harvesting capability. Figure 10a shows the schematic diagram for the heating and cooling setup used for pyroelectric energy harvesting. Two silicon oil beakers were initially maintained at 60 °C and 5 °C using a hot plate and chilled silicon oil. The

sample is manually moved in hot and cold oil beakers for cyclic temperature, current and voltage measurement. In the ~ 10 s/14 s, heating/cooling cycle (manually dipping sample in hot/cold silicon oil beakers alternatively) is performed, which provides ~ 6 – 7 °C temperature variation as shown in Fig. 10b and the room temperature was ~ 32 °C. The material was heated from 32 to 39 °C in 10 s and then cooled back to 32 °C in 14 s, as shown in Fig. 10b. Here, it should be noted that the hot and cold bath temperature was 60 °C and 5 °C. The cycle temperature is obtained between 32 to 39 °C because of the frequency of the cycle, heat loss in the environment, and the mixing of hot and cold oil between beakers during the movement. The setup is made to analyze the present study. Thus, a more precise movement/frequency of the sample between the hot and cold beaker is needed to optimize or an automatic heating/cooling setup is required to obtain a smooth and higher temperature, current and voltage value. The current and voltage for pure and 2% NBT–6BT are shown in Fig. 10c and d. The peak (negative) to peak (positive) pyroelectric current (I) is ~ 15.5 nA and ~ 29 nA with 32–39 °C in 10 s for NBT–6BT and NBT–6BT (2% PMMA), respectively. Considering these data, if the pyroelectric coefficient is estimated using $p = (I/A) \times (dt/dT)$ (effective area of the coated sample was a diameter of 8.6 mm). Then, p is found as 3.69×10^{-4} C/m² (pure) and 6.9×10^{-4}

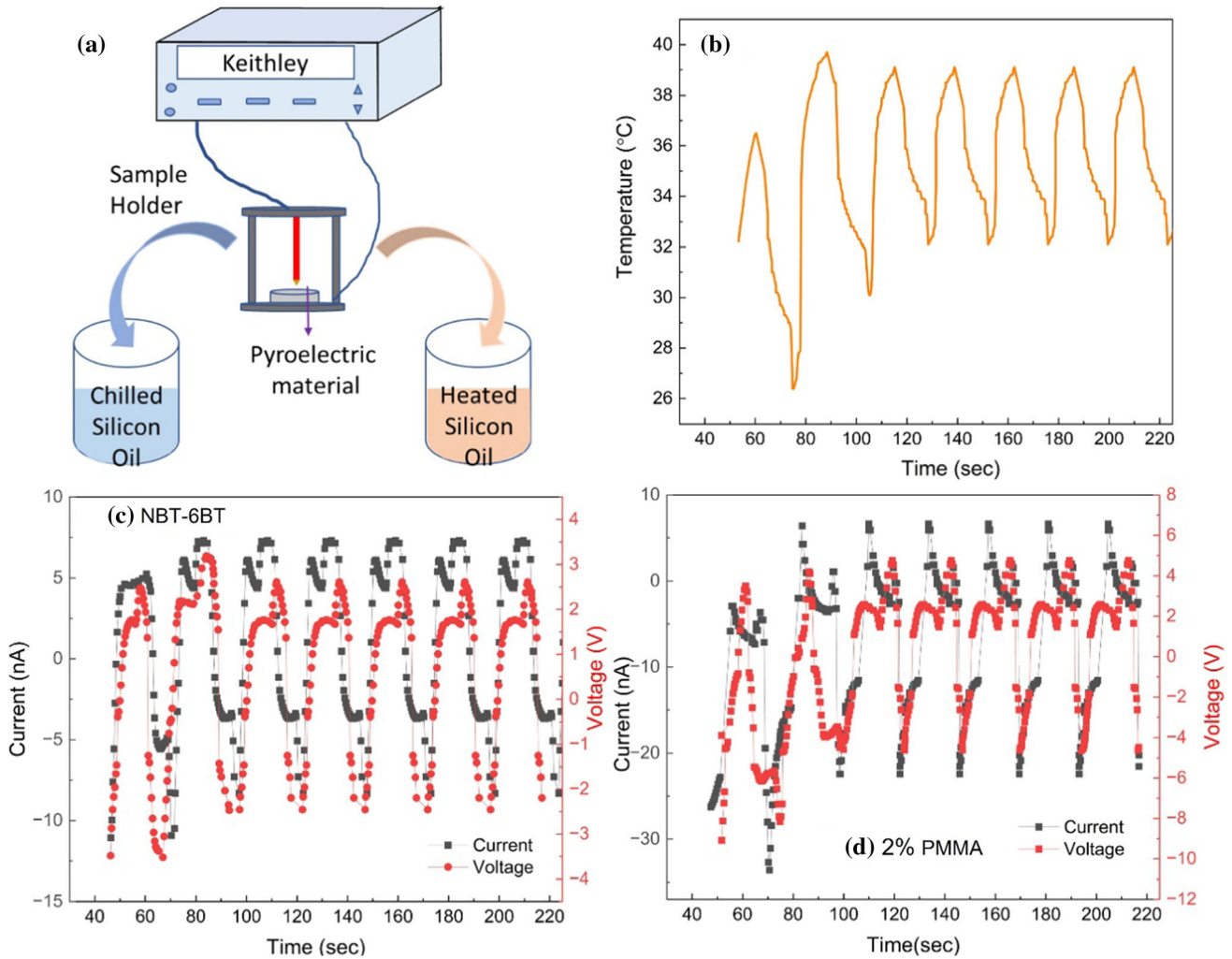


Figure 10 a Schematic diagram showing the pyroelectric energy harvesting using alternative heating and cooling, b variation of temperature with time; current and voltage variation for c NBT-6BT and d NBT-6BT (2% PMMA).

C/m² (2% PMMA), approximately the same as obtained by ramping as given in Table 1. Moreover, the peak (negative) to peak (positive) pyroelectric voltage (V) is ~ 5 V and 9.3 V for NBT-6BT and NBT-6BT (2% PMMA), respectively. The pyroelectric voltage and current in the porous sample are almost two orders higher than the pure NBT-6BT sample. Hence, the pyroelectric energy harvesting is ~ 4 orders higher than pure NBT-6BT; it is also confirmed by Table 1, where energy harvesting FOMs F_e and F_e^* are ~ 5–6 orders more than pure NBT-6BT.

Conclusion

Porous NBT-6BT demonstrated an enhanced pyroelectric property and figures of merit. The dielectric constant for pure NBT-6BT decreased from 2215 to 583 (8% PMMA) for unpoled samples and 790–373 for poled samples at room temperature. The p at room temperature for NBT-6BT (2% PMMA) showed an increment of 51% compared to pure NBT-6BT. The activation energy is independent of porosity. The porous material poling was ineffective with the increased pore size and porosity; hence, NBT-6BT (12% PMMA) could not be poled. The porous NBT-6BT (2% PMMA) material indicated an improved pyroelectric FOM at 30–80 °C. The energy harvesting FOM showed an increment of 186% at room temperature and 120.7% at 80 °C. The results

demonstrate the introduction of porosity in material to be an efficient technique for pyroelectric energy harvesting.

Acknowledgements

The authors thank Dr. Lalitha KV for providing the powder and measurement. S.P. also thanks Science and Engineering Research Board (SERB) for financial support in the frame of the Start-up Research Grant no. SRG/2020/000188. We are also grateful to Sophisticated Instrumentation Centre (SIC), IIT Indore for providing the characterization facility.

Author contribution

NS contributed to conceptualization, investigation, methodology and writing—original draft preparation; SP helped in writing—review and editing and supervising. All authors have read and agreed to the published version of the manuscript.

Data and code availability

The data that support the findings of this study are available within this article.

Declarations

Conflict of interest The authors declare that they have no known competing financial interests or personal relationships that could have influenced the work reported in this paper.

Ethical approval Not applicable.

References

- [1] Pandya S, Velarde G, Zhang L, Wilbur JD, Smith A, Hanrahan B, Dames C, Martin LW (2019) New approach to waste-heat energy harvesting: pyroelectric energy conversion. *NPG Asia Mater* 11:26
- [2] Lee FY, Navid A, Pilon L (2012) Pyroelectric waste heat energy harvesting using heat conduction. *Appl Therm Eng* 37:30–37
- [3] Siao A-S, McKinley IM, Chao C-K, Hsiao C-C, Pilon L (2018) Pyroelectric waste heat energy harvesting using the Olsen cycle on Pb(Zr, Ti)O₃-Pb(Ni, Nb)O₃ ceramics. *J Appl Phys* 124:174104
- [4] Tabbai Y, Hajjaji A, Moznine RE, Ennawaoui C, Belhora F, El Ballouti A (2018) Modeling of pyroelectric energy harvesting technology used for thermal sensing application. *Sens Lett* 16:211–216
- [5] Parida K, Bark H, Lee PS (2021) Emerging thermal technology enabled augmented reality. *Adv Funct Mater* 31:2007952
- [6] Whatmore RW, Ward SJ (2023) Pyroelectric infrared detectors and materials—a critical perspective. *J Appl Phys* 133:080902
- [7] Whatmore R (1986) Pyroelectric devices and materials. *Rep Prog Phys* 49:1335–1386
- [8] Cha G, Ji, Y, Ju Y S (2012) In: 2012 IEEE 25th International conference on micro electro mechanical systems (MEMS), IEEE, pp 1241–1244
- [9] Bowen CR, Taylor J, LeBoulbar E, Zabek D, Chauhan A, Vaish R (2014) Pyroelectric materials and devices for energy harvesting applications. *Energy Environ Sci* 7:3836–3856
- [10] Zhang D, Wu H, Bowen CR, Yang Y (2021) Recent advances in pyroelectric materials and applications. *Small* 17:2103960
- [11] Shen M, Li W, Li M-Y, Liu H, Xu J, Qiu S, Zhang G, Lu Z, Li H, Jiang S (2019) High room-temperature pyroelectric property in lead-free BNT-BZT ferroelectric ceramics for thermal energy harvesting. *J Eur Ceram Soc* 39:1810–1818
- [12] Patel S, Lalitha KV, Saurabh N (2022) Enhanced pyroelectric performance of lead-free Zn-doped Na_{1/2}Bi_{1/2}TiO₃-BaTiO₃ ceramics. *Materials* 15:87
- [13] Balakt AM, Shaw C, Zhang Q (2017) Large pyroelectric properties at reduced depolarization temperature in A-site nonstoichiometry composition of lead-free 0.94Na_xBi_yTiO₃-0.06 Ba₂TiO₃ ceramics. *J Mater Sci* 52:7382–7393. <https://doi.org/10.1007/s10853-017-0973-1>
- [14] Saurabh N, Patel S (2021) Nonstoichiometric effect on electrocaloric, pyroelectric and energy storage properties of 0.94Na_xBi_yTiO₃-0.06BaTiO₃ bulk ceramics. *J Mater Sci Mater Electron* 32:26871–26893
- [15] Mahdi R, Majid WA (2016) Piezoelectric and pyroelectric properties of BNT-base ternary lead-free ceramic-polymer nanocomposites under different poling conditions. *RSC Adv* 6:81296–81309
- [16] Shen M, Hu L, Li L, Zhang C, Xiao W, Zhang Y, Zhang Q, Zhang G, Jiang S, Chen Y (2021) High pyroelectric response over a broad temperature range in NBT-BZT: SiO₂ composites for energy harvesting. *J Eur Ceram Soc* 41:3379–3386

- [17] Batra A, Aggarwal M, Edwards ME, Bhalla A (2008) Present status of polymer: ceramic composites for pyroelectric infrared detectors. *Ferroelectr* 366:84–121
- [18] Kuruvila KM, Dhayanithi D, Manivannan S, Giridharan N, Vijayakumar P, Manikandan C, Sarguna R, Amaladass EP, Ganesamoorthy S, Varadarajan E (2022) A study on the electrical properties of flux grown 0.91PZN-0.09PT Single crystals for high-performance piezoelectric and pyroelectric device applications. *J Cryst Growth* 598:126875
- [19] Zhang G, Jiang S, Zeng Y, Zhang Y, Zhang Q, Yu Y (2009) High pyroelectric properties of porous $\text{Ba}_{0.67}\text{Sr}_{0.33}\text{TiO}_3$ for uncooled infrared detectors. *J Am Ceram Soc* 92:3132–3134
- [20] Zhang Y, Xie M, Roscow J, Bao Y, Zhou K, Zhang D, Bowen CR (2017) Enhanced pyroelectric and piezoelectric properties of PZT with aligned porosity for energy harvesting applications. *J Mater Chem A* 5:6569–6580
- [21] Zhang G, Jiang S, Zeng Y, Zhang Y, Zhang Q, Yu Y (2009) The modified model of the dielectric characteristics for porous $\text{Ba}_{0.6}\text{Sr}_{0.4}\text{TiO}_3$ ceramics. *J Appl Phys* 106:034110
- [22] Zhang Y, Bao Y, Zhang D, Bowen CR (2015) Porous PZT ceramics with aligned pore channels for energy harvesting applications. *J Am Ceram Soc* 98:2980–2983
- [23] Roscow J, Zhang Y, Taylor J, Bowen C (2015) Porous ferroelectrics for energy harvesting applications. *Eur Phys J Spec Top.* 224:2949–2966
- [24] Aggarwal M, Kumar M, Syal R, Singh V, Singh AK, Dhimman S, Kumar S (2020) Enhanced pyroelectric figure of merits in Sr and Zr co-doped porous BaTiO_3 ceramics. *J Mater Sci Mater Electron* 31:2337–2346
- [25] Srikanth K, Singh V, Vaish R (2017) Enhanced pyroelectric figure of merits of porous $\text{BaSn}_{0.05}\text{Ti}_{0.95}\text{O}_3$ ceramics. *J Eur Ceram Soc* 37:3943–3950
- [26] Sharma M, Singh V, Singh S, Azad P, Ilahi B, Madhar NA (2018) Porous $\text{Ba}_{0.85}\text{Ca}_{0.15}\text{Zr}_{0.1}\text{Ti}_{0.9}\text{O}_3$ ceramics for pyroelectric applications. *J Electron Mater* 47:4882–4891
- [27] Hiruma Y, Nagata H, Takenaka T (2009) Thermal depoling process and piezoelectric properties of bismuth sodium titanate ceramics. *J Appl Phys* 105:084112
- [28] Zhou X, Xue G, Luo H, Bowen CR, Zhang D (2021) Phase structure and properties of sodium bismuth titanate lead-free piezoelectric ceramics. *Prog Mater Sci* 122:100836
- [29] Bremecker D, Slabki M, Koruza J, Rödel J (2022) Characterization of crystal structure, electrical and electromechanical properties of Mg-doped $0.94\text{Na}_{1/2}\text{Bi}_{1/2}\text{TiO}_3-0.06\text{BaTiO}_3$. *J Eur Ceram Soc* 42:5591–5597
- [30] Jo W, Daniels J, Damjanovic D, Kleemann W, Rödel J (2013) Two-stage processes of electrically induced-ferroelectric to relaxor transition in $0.94(\text{Bi}_{1/2}\text{Na}_{1/2})\text{TiO}_3-0.06\text{BaTiO}_3$. *Appl Phys Lett* 102:192903
- [31] Turki O, Slimani A, Sassi Z, Khemakhem H, Abdelmoula N, Lebrun L (2022) Effect of sintering temperature of NBT–6BT lead-free ceramics on the structural, ferroelectric and piezoelectric properties. *Appl Phys A* 128:186
- [32] Zhu S, Cao L, Xiong Z, Lu C, Gao Z (2018) Enhanced piezoelectric properties of 3–1 type porous $0.94\text{Bi}_{0.5}\text{Na}_{0.5}\text{TiO}_3-0.06\text{BaTiO}_3$ ferroelectric ceramics. *J Eur Ceram Soc* 38:2251–2255
- [33] Seo I-T, Steiner S, Frömling T (2017) The effect of A site non-stoichiometry on $0.94(\text{Na}_y\text{Bi}_x)\text{TiO}_3-0.06\text{BaTiO}_3$. *J Eur Ceram Soc* 37:1429–1436
- [34] Zeng T, Dong X, Mao C, Zhou Z, Yang H (2007) Effects of pore shape and porosity on the properties of porous PZT 95/5 ceramics. *J Eur Ceram Soc* 27:2025–2029
- [35] Yan M, Xiao Z, Ye J, Yuan X, Li Z, Bowen C, Zhang Y, Zhang D (2021) Porous ferroelectric materials for energy technologies: current status and future perspectives. *Energy Environ Sci* 14:6158–6190
- [36] Wohmsland A, Fetzer A-K, Riaz A, Kleebe H-J, Rödel J, Kodumudi Venkataraman L (2021) Correlation between enhanced lattice distortion and volume fraction of polar nanoregions in quenched $\text{Na}_{1/2}\text{Bi}_{1/2}\text{TiO}_3-\text{BaTiO}_3$ ceramics. *Appl Phys Lett* 118:072903
- [37] Wang X, Venkataraman LK, Tan C, Li Y (2021) Fracture behavior in electrically poled alkaline bismuth-and potassium-based lead-free piezoceramics using Vickers indentation. *Scripta Mater* 194:113647
- [38] Zhang H, Li J-F, Zhang B-P (2007) Microstructure and electrical properties of porous PZT ceramics derived from different pore-forming agents. *Acta Mater* 55:171–181
- [39] Anton E-M, Jo W, Damjanovic D, Rödel J (2011) Determination of depolarization temperature of $(\text{Bi}_{1/2}\text{Na}_{1/2})\text{TiO}_3$ -based lead-free piezoceramics. *J Appl Phys* 110:094108
- [40] Woodward DI, Dittmer R, Jo W, Walker D, Keeble DS, Dale MW, Rödel J, Thomas PA (2014) Investigation of the depolarisation transition in Bi-based relaxor ferroelectrics. *J Appl Phys* 115:114109
- [41] Sapper E, Schaab S, Jo W, Granzow T, Rödel J (2012) Influence of electric fields on the depolarization temperature of Mn-doped $(1-x)\text{Bi}_{1/2}\text{Na}_{1/2}\text{TiO}_3-x\text{BaTiO}_3$. *J Appl Phys* 111:014105
- [42] Kodumudi Venkataraman L, Zhu T, Pinto Salazar M, Hofmann K, Iqbal Waidha A, Jaud J, Groszewicz PB, Rödel J (2021) Thermal depolarization and electromechanical hardening in Zn^{2+} -doped $\text{Na}_{1/2}\text{Bi}_{1/2}\text{TiO}_3-\text{BaTiO}_3$. *J Am Ceram Soc* 104:2201–2212
- [43] Slabki M, Venkataraman LK, Rojac T, Rödel J, Koruza J (2021) Thermal stability of the electromechanical properties in acceptor-doped and composite-hardened $(\text{Na}_{1/2}\text{Bi}_{1/2})\text{TiO}_3-\text{BaTiO}_3$ ferroelectrics. *J Appl Phys* 130:014101

- [44] Bai W, Chen D, Zheng P, Shen B, Zhai J, Ji Z (2016) Composition-and temperature-driven phase transition characteristics and associated electromechanical properties in $\text{Bi}_{0.5}\text{Na}_{0.5}\text{TiO}_3$ -based lead-free ceramics. *Dalton Trans* 45:8573–8586
- [45] Hinterstein M, Schmitt L, Hoelzel M, Jo W, Rödel J, Kleebe H-J, Hoffman M (2015) Cyclic electric field response of morphotropic $\text{Bi}_{1/2}\text{Na}_{1/2}\text{TiO}_3$ - BaTiO_3 piezoceramics. *Appl Phys Lett* 106:222904
- [46] Craciun F, Galassi C, Birjega R (2012) Electric-field-induced and spontaneous relaxor-ferroelectric phase transitions in $(\text{Na}_{1/2}\text{Bi}_{1/2})_{1-x}\text{BaxTiO}_3$. *J Appl Phys* 112:124106
- [47] Newnham R, Skinner D, Cross L (1978) Connectivity and piezoelectric-pyroelectric composites. *Mater Res Bull* 13:525–536
- [48] Lang SB, Das-Gupta DK (2001) Pyroelectricity: Fundamentals and applications. In: Nalwa HS (ed) *Handbook of advanced electronic and photonic materials and devices*. Elsevier, Amsterdam, pp 1–55
- [49] Balakt AM, Shaw CP, Zhang Q (2017) Giant pyroelectric properties in La and Ta co-doped lead-free $0.94\text{Na}_{0.5}\text{Bi}_{0.5}\text{TiO}_3$ - 0.06BaTiO_3 ceramics. *J Alloy Compd* 709:82–91
- [50] Liu X, Wu D, Chen Z, Fang B, Ding J, Zhao X, Luo H (2015) Ferroelectric, dielectric and pyroelectric properties of Sr and Sn codoped BCZT lead free ceramics. *Adv Appl Ceram* 114:436–441
- [51] Lau ST, Cheng C, Choy S, Lin D, Kwok KW, Chan HL (2008) Lead-free ceramics for pyroelectric applications. *J Appl Phys* 103:104105

Publisher's Note Springer Nature remains neutral with regard to jurisdictional claims in published maps and institutional affiliations.

Springer Nature or its licensor (e.g. a society or other partner) holds exclusive rights to this article under a publishing agreement with the author(s) or other rightsholder(s); author self-archiving of the accepted manuscript version of this article is solely governed by the terms of such publishing agreement and applicable law.